3952–3963 *Nucleic Acids Research, 2012, Vol. 40, No. 9* *Published online 16 January 2012*
doi:10.1093/nar/gks008

Complex activities of the human Bloom's syndrome helicase are encoded in a core region comprising the RecA and Zn-binding domains

Máté Gyimesi[1], Gábor M. Harami[1], Kata Sarlós[1], Eszter Hazai[2], Zsolt Bikádi[2] and Mihály Kovács[1,*]

[1]Department of Biochemistry, ELTE-MTA 'Momentum' Motor Enzymology Research Group, Eötvös University, Pázmány P. s. 1/c, H-1117 Budapest and [2]VirtuaDrug Ltd, Csalogány u. 4/C, H-1015 Budapest, Hungary

Received September 27, 2011; Revised December 23, 2011; Accepted January 3, 2012

ABSTRACT

Bloom's syndrome DNA helicase (BLM), a member of the RecQ family, is a key player in homologous recombination (HR)-based error-free DNA repair processes. During HR, BLM exerts various biochemical activities including single-stranded (ss) DNA translocation, separation and annealing of complementary DNA strands, disruption of complex DNA structures (e.g. displacement loops) and contributes to quality control of HR via clearance of Rad51 nucleoprotein filaments. We performed a quantitative mechanistic analysis of truncated BLM constructs that are shorter than the previously identified minimal functional module. Surprisingly, we found that a BLM construct comprising only the two conserved RecA domains and the Zn^{2+}-binding domain (residues 642–1077) can efficiently perform all mentioned HR-related activities. The results demonstrate that the Zn^{2+}-binding domain is necessary for functional interaction with DNA. We show that the extensions of this core, including the winged-helix domain and the strand separation hairpin identified therein in other RecQ-family helicases, are not required for mechanochemical activity *per se* and may instead play modulatory roles and mediate protein–protein interactions.

INTRODUCTION

Most genomes are built up from stable, double-stranded (ds) forms of DNA or RNA. This arrangement necessitates enzymatic unwinding of the two strands to access and manipulate the encoded information. Helicases are ubiquitous NTPases capable of separating complementary strands of nucleic acids. Beside those playing roles in replication, multiple groups of DNA helicases have specialized functions in DNA repair (1). Members of the RecQ helicase family [part of superfamily (SF) 2] are essential in homologous recombination (HR)-based error-free DNA repair processes in all kingdoms of life. The human genome encodes five RecQ family helicases termed RecQ1, BLM, WRN, RecQ4 and RecQ5. Three of these paralogues are affected in genetic diseases: BLM in Bloom's syndrome, WRN in Werner's syndrome and RecQ4 (RTS) in Rothmund–Thomson syndrome. BLM plays genome-wide roles in HR-mediated repair of double-stranded DNA breaks (DSBs), one of the most serious genetic disintegrities (2). In the early stages of HR, BLM assists the resection of the 5′-DNA end at DSB sites (3,4), and exerts quality control functions by disrupting human (h) Rad51 nucleoprotein filaments and/or promoting strand exchange (5,6) (Supplementary Figure S1). Once HR has passed through this stage, BLM performs numerous further activities, which drive HR towards the formation of non-crossover products (1). The 'early' and 'late' HR functions of BLM were recently demonstrated *in vivo* in mouse embryonic stem cells (7). The mechanochemical activities of BLM utilized in HR span from the ability to translocate along single-stranded (ss) DNA and unwind or anneal complementary DNA strands, to the disruption of displacement loops (D-loops) and nucleoprotein filaments, and dissolution of double Holliday junctions (DHJs).

It is reasonable to surmise that the above complex activities require complex protein structure. Indeed, BLM is a multidomain protein consisting of seven distinct structural regions. BLM was shown to form oligomeric (hexa- or tetrameric) structures in the absence of DNA (8). The N-terminal part of BLM ($BLM^{1–431}$) was shown to exist as hexa- and dodecamers (9), suggesting that the large N-terminal domain (amino acid residues 1–641) promotes oligomerization. Moreover, the N-terminal domain was shown to provide binding sites for numerous partner proteins (10–16). Deletion of this domain abolished BLM oligomerization, but it did not

*To whom correspondence should be addressed. Tel: +36 1 372 2500 (extn. 8401); Fax: +36 1 381 2172; Email: kovacsm@elte.hu

affect its enzymatic activities (17,18). Similarly, to other SF2 and SF1 helicases, BLM has two tandem (N- and C-core) RecA domains (amino acids 642–993), which form the ATP binding site, contribute to DNA binding and drive inchworm-like movement along DNA. The family-specific RecQ C-terminal region (RQC) comprises the Zn^{2+}-binding domain (ZnBD, amino acids 994–1068) and the winged-helix domain (WH, amino acids 1069–1189), which play roles in proper folding and DNA and protein binding, respectively (18–22). The contribution of the ZnBD and WH domains to the binding of DNA substrates is suggested by the finding that an isolated RQC construct had similar affinities to fork, G4 and HJ substrates to those of full-length BLM (20). The helicase and RNase D C-terminal domain (HRDC, amino acids 1190–1290) has auxiliary DNA-binding roles (18). The C-terminal region (amino acids 1291–1417), which is probably unstructured, plays roles in protein–protein interactions and encompasses the nuclear localization signal (2).

The RecA region of various SF1 and SF2 helicases harbours a β-hairpin motif that was identified as a key structural element promoting DNA strand separation. This pin (referred to as RecA-pin in this article) is located in the C-core RecA domain of helicases unwinding in the 3′–5′ direction [including PcrA (23), Rep (24), UvrD (25) and Hel308 (26)], whereas it can be found in the N-core domain of RecD2, a 5′–3′ helicase (27). All mentioned helicases harbour an aromatic residue at the tip of this pin, similarly to *E. coli* (Ec) RecQ (F221, PDB structure 1OYY) (28). Interestingly, neither BLM nor RecQ1 possess an aromatic side chain in the homologous position (29).

Within the ZnBD of BLM, four conserved cysteine residues (C1036, C1055, C1063, C1066) and a salt bridge-forming side chain pair (R1038–D1064) have been shown to be essential for Zn^{2+}-dependent correct folding and functioning of the enzyme (18,19,21). In line with characterized *in vitro* mutations affecting these residues, genetic variants of C1055 and D1064 have been identified as Bloom's syndrome-causing mutations (30). Another structural element of the ZnBD, a helical hairpin (referred to as ZnBD-pin), has been proposed to play a role in unwinding by leading the newly separated DNA strand to the RecA motor core of human RecQ1 and WRN helicases (29,31).

The WH domain of RecQ1 harbours a hairpin motif essential for DNA unwinding via the protrusion of an essential aromatic residue (Y564), as evidenced by mutational analysis and crystallography (PDB code 2WWY) (29,32). The crystal structure of the dsDNA-bound WH domain of WRN revealed the existence of a homologous β-hairpin with an aromatic residue at its tip (F1037; PDB code 3AAF) (31). This pin (referred to as WH-pin) displaces the terminal nucleotide unit of the DNA ligand, supporting its unwinding role also in WRN. Contrary, mutations within the corresponding region of EcRecQ did not affect DNA unwinding, indicating that the WH-pin may not be universally essential for RecQ-family helicase activity (29).

A truncated version of EcRecQ (amino acids 1–524) lacking the HRDC domain unwound dsDNA as effectively as the wild-type protein (29). However, a similar construct used for crystallography (amino acids 1–516) (28) showed reduced ssDNA binding (33,34). A short splice form of *Drosophila* RecQ5, which naturally lacks the HRDC domain, also had unwinding activity similar to a longer, HRDC-containing splice form (35). Human RecQ1 also lacks the HRDC domain but possesses unwinding activity (36). A HRDC-deleted mutant (amino acids 1–1119) of Sgs1, the yeast homologue of BLM, was insoluble, while another construct containing the HRDC domain (amino acids 400–1268) was soluble and retained the activity profile of full-length Sgs1 (37). A plant RecQ helicase from *Arabidopsis thaliana* (AtRecQ3), naturally lacking the WH and HRDC domains, has recently been shown to be capable of annealing complementary DNA strands, unwinding nicked HJs, but unable to migrate intact HJs (38). Interestingly, another RecQ helicase from the same organism (AtRecQ1) consists of only the two RecA domains and the ZnBD (39), but its biochemical properties are unexplored. Taken together, the above findings suggest that the HRDC domain, while its presence is important for some functions, is not essential for the mechanochemical activity of RecQ helicases in general.

Truncation of the C-terminal part of BLM's HRDC domain (construct comprising amino acids 213–1267) resulted in defects in strand annealing (17) as well as DHJ-binding and -dissolution activities (40), while the dsDNA unwinding activity remained unchanged (17,40). Another construct harbouring an intact HRDC domain and C-terminal region (amino acids 642–1417) retained DHJ dissolution activity, indicating the role of the HRDC domain in this process (40). A BLM construct comprising the regions homologous to EcRecQ (BLM amino acids 642–1290, referred to as BLM^{1290} in this article) retained the ATPase and DNA unwinding activities and DNA substrate specificity profile of the full-length enzyme (BLM^{FL}) (18,41). However, the ability of BLM^{1290} to form higher-order protein–DNA complexes and catalyse DNA strand annealing was significantly reduced (17). In contrast to BLM^{1290}, the strand annealing activity of a slightly longer construct (amino acids 642–1350) was similar to that of BLM^{FL} (17). These findings suggested that the region between residues 1290 and 1350 is required for strand annealing. Further truncation of the entire HRDC domain (construct comprising amino acids 642–1108) resulted in defects in ssDNA binding in mobility shift experiments (18). This construct was also unable to bind to heparin column during protein preparation, again indicative of impaired DNA binding (18). In line with these data, a point mutation in the HRDC domain of BLM (S1209T) causes Bloom's syndrome (30). Moreover, another single substitution in the HRDC domain (K1270V) was shown to affect DHJ dissolution (40). Interestingly, RecQ1 and WRN possess Lys at this position, similarly to BLM, but cannot dissolve DHJ structures (40).

To identify the structural elements that are essential for the various mechanochemical activities of BLM, in the

present study we compared the mechanistic properties of the previously investigated BLM^{FL} and BLM^{1290} constructs with those of new constructs that are shorter than previously characterized ones. These include BLM amino acids 642–1005 (referred to as BLM^{1005}) comprising solely the two RecA-core domains, and BLM amino acids 642–1077 (BLM^{1077}) consisting of the RecA cores and the ZnBD (Figure 1). Surprisingly, we found that BLM^{1077} retains all of the ATPase, ssDNA translocation and dsDNA unwinding activities, exhibiting highly similar mechanistic parameters to those of BLM^{1290}. The results demonstrate that the RecA domains and the ZnBD comprise a minimal functional helicase core even in the absence of the WH domain that was proposed to be the strand-separating unit of other RecQ helicases (29,31,32). In addition, BLM^{1077} exhibits more pronounced strand annealing than BLM^{1290}, which shows that previously implicated C-terminal regions are not essential for this activity. We also demonstrate that BLM^{1077} is capable of disrupting D-loop structures and it has an enhanced capability for nucleoprotein disassembly.

MATERIALS AND METHODS

Reagents

Unless otherwise stated, all reagents were from Sigma–Aldrich Co. ATP and adenosine 5′-(β,γ-imido)triphosphate (AMPPNP) were from Roche Applied Science. Phosphate (P_i) standard solution was from Merck. m13mp18 ssDNA isolation was carried out as in (42). Oligonucleotides were from VBC-Biotech (Supplementary Table S1). Except where stated, DNA concentrations are expressed as those of oligo- or polynucleotide molecules (as opposed to those of constituent nucleotide units). All measurements were carried out at 25°C. Data analysis was performed using OriginLab 8.0 and KinTek SF-2004 software.

Cloning

The coding regions of BLM^{1005} and BLM^{1077} were amplified by PCR from the pTXB3/$BLM^{642–1290}$ plasmid (41) and subcloned between the NcoI and SapI sites of pTXB3 (New England Biolabs). All constructs were verified by DNA sequencing.

Protein purification

BLM^{FL} was expressed as previously described (43) with some modifications as follows. *Saccharomyces cerevisiae* cells (JEL1 strain) containing pYES2/BLM-His_6 were grown in selective media (containing 3% (v/v) glycerol and 2% (v/v) DL-lactate in the absence of sugar) at 30°C. After 24-h expression at 20°C, cells were frozen in liquid N_2 in large bullets and quickly ground in a coffee grinder. The cell powder was then melted in a water bath. Subsequent steps were done as described in (43). The purified protein was frozen and stored in liquid N_2 in 40-µl droplets.

BLM^{1290}, BLM^{1077} and BLM^{1005} were expressed and purified as described previously for BLM^{1290} (41). Coumarin-labelled P_i-binding protein (MDCC-PBP) and hRad51 were prepared as described in refs (44) and (45), respectively.

Escherichia coli single-stranded DNA binding protein (SSB) was expressed and purified as previously described in (46) with the following modifications. *Escherichia coli* B ER2566 strain was used to express SSB in 4-l 2YT medium. Triton X-100 (0.1%) was used in the Lysis buffer instead of deoxycholate. Expression was induced at $OD_{600} = 0.3$ with 1 mM IPTG and cell were shaken for 16 h at 18°C. Lysozyme treatment was carried out at 4°C for 1 h. After ammonium sulphate precipitation and dialysis against HP buffer [50 mM Tris–HCl pH 7.5, 50 mM NaCl, 0.1 mM EDTA, 1 mM DTT, 10% (v/v) glycerol], SSB was loaded onto a HiTrap Heparin HP column and eluted with a linear NaCl gradient (50 mM–2 M) in HP buffer. After pooling fractions containing SSB, ammonium sulphate precipitation was

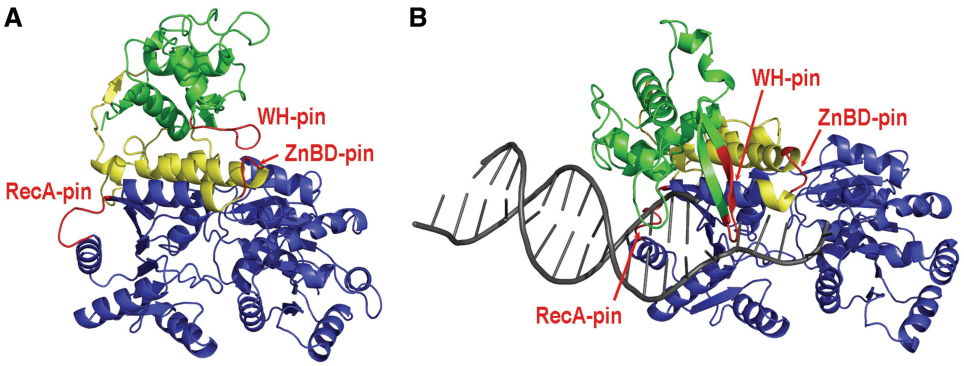

Figure 1. Homology model-based representation of the BLM segment comprising the RecA, ZnBD and WH domains. Shown are homology-modelled structures of BLM in two different conformations, determined crystallographically for EcRecQ (1OYY, **A**) and human RecQ1 (2WWY, **B**). Protein segments present in BLM^{1005} (comprising the two RecA domains) are shown in blue, whereas the additional segment present in BLM^{1077} (including the ZnBD) is shown in yellow. The green segment (WH domain) is missing from both BLM^{1005} and BLM^{1077}, but is present in BLM^{1290} and BLM^{FL}. Pin-like elements implicated in DNA strand separation in various helicases are shown in red. The bound DNA present in the 2WWY-based model is shown in grey.

repeated. Purified SSB was dialysed against Storage buffer (50 mM Tris–HCl pH 7.5, 200 mM NaCl, 1 mM DTT, 10% (v/v) glycerol) and frozen in liquid N_2 in small droplets.

MDCC-SSB labelling and preparation were done by the method described for IDCC-SSB in (47), with the following modifications. MDCC (*N*-[2-(1-maleimidyl) ethyl]-7-diethylaminocoumarin-3-carboxamide) (Invitrogen) was used instead of IDCC (*N*-[2-(iodoacetamido) ethyl]-7-diethylaminocoumarin-3-carboxamide), and the labelling reaction was performed for 3 h under argon gas. The labelled protein was isolated by passing through a PD10 (GE Healthcare) gel filtration column, pre-equilibrated with a buffer containing 50 mM Tris–HCl pH 7.5, 200 mM NaCl, 1 mM DTT and 10% glycerol. Protein concentration was measured according to Bradford's method with bovine serum albumin as standard. MDCC content was measured by coumarin absorbance at 430 nm using $\varepsilon_{430} = 46\,800\,M^{-1}cm^{-1}$. The labelled protein was stored in liquid nitrogen.

Steady-state kinetics

ATPase activities were measured using a pyruvate kinase/lactate dehydrogenase (PK/LDH) coupled assay (14 U/ml PK, 20 U/ml LDH, 1 mM ATP, 1 mM phosphoenol pyruvate, 200 μM NADH) in SF-50 buffer (50 mM Tris–HCl pH 7.5, 50 mM NaCl, 5 mM $MgCl_2$, 1 mM DTT) containing 50 μg/ml BSA. NADH absorbance was followed at 340 nm in a Shimadzu UV-2101PC spectrophotometer, and ATPase activities were calculated from linear fits to NADH absorbance changes ($\varepsilon_{340} = 6220\,M^{-1}cm^{-1}$).

Transient kinetics

Single-round translocation experiments were carried out in a KinTek SF-2004 stopped-flow apparatus in the presence of heparin as protein trap, and nucleoprotein displacement experiments were carried out in a BioLogic SFM 300/400 stopped-flow apparatus. Post-mix concentrations are stated. P_i release measurements were performed in SF-50 buffer. P_i mop (150 μM 7-methylguanosine, 0.1 U/ml purine nucleoside phosphorylase) and 3 μM MDCC-PBP were present in all solutions. MDCC-PBP and MDCC-SSB fluorescence was excited at 436 nm, and emission was followed by using a 455-nm long path filter (Comar Optics). MDCC-PBP fluorescence calibration was carried out as described earlier (41). Heparin (Sigma H3393) was dissolved in sterile distilled water at 50 mg/ml and prior to measurements it was dialysed against sterile distilled water and then SF-50 buffer (in MWCO 3500 dialysis tubing; Serva 44183).

Electrophoretic assays

DNA substrates (3 nM, listed in Supplementary Table S1) were used in unwinding, annealing and D-loop disruption assays. Reaction volume was 10 μl in Buffer-H (30 mM Tris–HCl pH 7.5, 100 mM KCl, 1 mM DTT, 10 μg/ml BSA, 20 mM creatine phosphate, 20 μg/ml creatine kinase) containing 2 mM ATP (absent in annealing assays) and 2.4 mM $MgCl_2$. Samples were mixed on ice, and the reaction was started with the addition of helicase (0–1 μM) and incubated at 37°C for 15 min. Reactions were stopped by the addition of loading dye (10 mM Tris–HCl pH 7.5, 60 mM EDTA, 60% glycerol, 0.075% Orange G) containing 0.83% SDS and 1.67 mg/ml proteinase K. Mixtures were incubated at 37°C for additional 3 min. Samples were then loaded on non-denaturing polyacrylamide gels in TBE buffer (89 mM Tris–HCl pH 7.5, 89 mM boric acid, 20 mM EDTA). Electrophoresis was carried out at 4°C. Fluorescently labelled DNA was detected using a Typhoon TRIO+ Variable Mode Imager (Amersham Biosciences).

Homology modelling

For sequence alignments and homology models comprising the RecA, ZnBD and WH domains of BLM, we used the BLM primary sequence with Universal Protein Resource accession code P54132, and the experimentally determined atomic structures of EcRecQ bound to ATPγS [PDB code 1OYY, similar to 1OYW (28)], human RecQ1 complexed with DNA [2WWY, similar to 2V1X (29)], and the WH domain of human WRN bound to DNA [3AAF (31)]. Structure-based sequence alignment (Supplementary Figure S2) of the templates and BLM was carried out using Staccato program, which uses structural alignment information to improve the quality of sequence alignments (48). The RecA-ZnBD and WH regions of BLM as well as 1OYY and 2WWY templates were separated during the alignment process, due to different relative conformations of these regions in 1OYY and 2WWY. Based on this alignment, we built BLM homology models in the two different available RecQ helicase conformations based on templates 1OYY and 2WWY, respectively. 3D atomic models comprising all non-hydrogen atoms were generated by the Modeller9.8 package (49) using refine.very slow option for simulated annealing. Heteroatoms (Zn, ATPγS, DNA) were included in model building. A bundle of 10 models from random generation of the starting structures was calculated in both cases. The models possessing the lowest DOPE score were chosen for further analysis. The qualities of the models were evaluated using Procheck (50). The percentage of residues found in the allowed regions of the Ramachandran diagram were 99.2 and 99.5% for 1OYY- and 2WWY-based models, respectively.

RESULTS

Construct design

We created homology models of BLM based on structure-based sequence alignments of the crystallographically determined atomic structures of the protein segments comprising the RecA, ZnBD and WH domains of EcRecQ (1OYY) (28) and human RecQ1 (2WWY) (29) (Figure 1, Supplementary Figure S2, pdb files provided in Supplementary Data). These structures represent two different conformations of this helicase segment in which the WH domain adopts different positions relative to the other domains. In the alignments, we also used the sequence and atomic structure of the WH domain

of human WRN (3AAF) (31). The 1OYY-based BLM structure was similar to an earlier model based on the same structure (19), with differences confined mainly to loop regions. Using the above models, we designed truncated BLM constructs to identify the minimal functional core of the enzyme. The BLM^{1005} construct consists solely of the two RecA domains, whereas BLM^{1077} contains the ZnBD in addition to the RecA domains (Figure 1). We compared the properties of these constructs to those of BLM^{1290} (comprising also the WH and HRDC domains) and BLM^{FL}.

The ZnBD is essential for normal functioning of BLM

The preparation yield of BLM^{1005} was only ~5% of that of BLM^{1290}, because most of the expressed protein was insoluble. The basal (DNA-free) ATPase activity of the soluble fraction of BLM^{1005} was $k_{basal,1005} = 0.02 \pm 0.01\,s^{-1}$, well below that of BLM^{1290} and BLM^{FL} [$k_{basal,1290} = 0.08 \pm 0.01\,s^{-1}$ $k_{basal,FL} = 0.22 \pm 0.08\,s^{-1}$; cf. Ref. (41)]. More importantly, ssDNA activation of BLM^{1005} ATPase was not detectable, in contrast to all other examined constructs (see below). These results showed that the two RecA domains alone are insufficient for correct folding and functioning of BLM.

The expression yield of BLM^{1077} was similar to that of BLM^{1290}. In contrast to earlier results on the longer $BLM^{642–1108}$ construct (18), BLM^{1077} bound to the heparin column similarly to BLM^{1290} and eluted at a similar NaCl concentration (300 mM), suggesting that its general DNA binding propensity was not altered significantly by the deletion of the WH and HRDC domains. Moreover, both its basal ($k_{basal,1077} = 0.27 \pm 0.06\,s^{-1}$) and DNA-activated ATPase activities suggested that BLM^{1077} folded properly and retained normal functioning characteristic of the longer constructs (Supplementary Figure S3). The steady-state K_{DNA} values (DNA concentrations required for half-maximal ATPase activation) of BLM^{1077} were similar to those of BLM^{FL} and BLM^{1290}, again indicating similar DNA interaction properties of the constructs (Supplementary Figure S3).

BLM^{1077} shows unaffected ssDNA translocation processivity and mechanochemical coupling

To test the ssDNA translocation activity of BLM^{1077}, we measured the dependence of its steady-state ATPase k_{cat} on oligo-dT substrate length (Figure 2; lengths expressed in nucleotide units). Similarly to our earlier findings on BLM^{1290} (41), BLM^{1077} showed two characteristic features: the steady-state k_{cat} values increased and showed saturation with increasing DNA length, whereas the K_{DNA} values showed a drastic length dependence <10 nt [delineating the binding site size (*b*) of the helicase], and stagnated above this length. Analysis of the data confirmed that BLM^{1077} actively translocates along the ssDNA track, with slightly higher ATPase rates both during translocation (k_{trans}) and at the 5′-end (k_{end}) than BLM^{1290} (Table 1) (41). Dissociation from the 5′-end ($k_{off,end}$) was also accelerated compared to BLM^{1290}, resulting in saturation of k_{cat} values at shorter

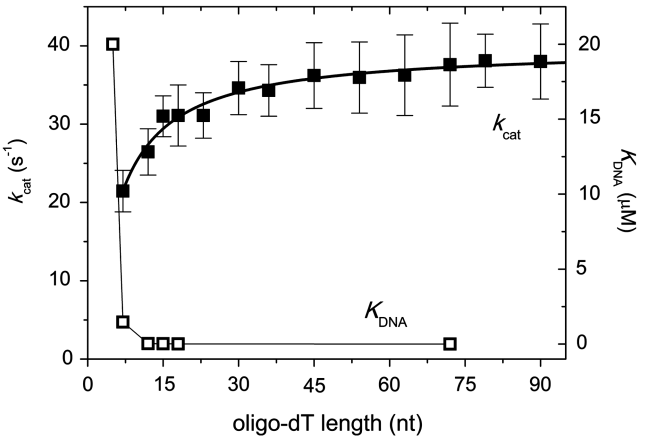

Figure 2. DNA length-dependent ATPase kinetics indicate active ssDNA translocation by BLM^{1077}. Shown are steady-state ATPase k_{cat} (filled square) and K_{DNA} (open square, ssDNA concentration required for half-maximal activation) values of 20 nM BLM^{1077} in the presence of oligo-dT substrates of different length at 25°C. k_{cat} values were fitted (solid line) with the equation described previously for BLM^{1290} (41). Determined mechanistic parameters are listed in Table 1. The break point in K_{DNA} values indicated a binding site size (*b*) of ~10 nt, which is detectably smaller than that previously described for BLM^{1290} (~14 nt) (41). See Supplementary Figure S3 for comparison of ATPase profiles of BLM^{1077} with those of BLM^{1290} and BLM^{FL} in the presence of DNA substrates of different structure. Error bars represent SEM in all figures.

DNA lengths. The data also indicated that the step size (*s*) remained 1 nt/ATP. However, this parameter was less robust due to the relatively small difference between k_{trans} and k_{end} and the high $k_{off,end}$ value.

To determine the translocation processivity of BLM^{1077}, we measured the kinetics of P_i production form ATP in single-round translocation conditions in the presence of oligo-dT substrates of different length (Figure 3). Heparin was used as a protein trap to achieve single-round conditions. Heparin turned out to be an efficient trap for BLM^{1077}, because it blocked the rebinding of DNA to the dissociated helicase, while it did not significantly enhance its DNA-free ATPase activity (Figure 3 and Supplementary Figure S4). As we described earlier for BLM^{1290} (41), upon mixing BLM^{1077} plus oligo-dT substrate with ATP plus heparin, the experimental traces showed multiphasic profiles. A first pre-steady-state exponential burst (Supplementary Figure S4) was followed by two other distinct phases corresponding to ATPase cycling during translocation along DNA and in the dissociated (trap-bound) state of the enzyme, respectively. The existence of a pre-steady-state exponential burst corresponding to a single ATP turnover by BLM^{1077} [identical to that by BLM^{1290} (41)] suggested that the rate-limiting step in the ATPase cycle during translocation was not changed by the truncation. The ATPase rate during the translocation-based phase was in good agreement with that determined using the PK/LDH-coupled ATPase assay (Figures 2 and 3; Supplementary Figure S4 and Table 1). The DNA length dependence of the amplitude of P_i production during translocation can be utilized to determine the mechanochemical coupling stoichiometry

Table 1. Kinetic parameters of BLM^{1077} compared to those of BLM^{1290}

		Method of determination	BLM^{1077}	BLM^{1290a}
k_{basal}	Steady-state ATPase activity in the absence of DNA (s^{-1})	PK/LDH assay	0.27 ± 0.06	0.08 ± 0.01
k_{trans}	Steady-state ATPase activity during ssDNA translocation (s^{-1})	PK/LDH assay	40 ± 5	33 ± 2
		MDCC-PBP	35 ± 1	27 ± 2
k_{end}	Steady-state ATPase activity at 5′-end of ssDNA (s^{-1})	PK/LDH assay	24 ± 7	5.6 ± 0.5
$k_{off,end}$	Dissociation from 5′-end of ssDNA (s^{-1})	PK/LDH assay	7 ± 3	2.7 ± 0.3
b	Binding site size (nt)	PK/LDH assay, MDCC-PBP	~10	~14
C	Coupling stoichiometry (ATP/nt)	MDCC-PBP	0.83 ± 0.11	0.87 ± 0.08
s	Step size during translocation (nt/ATP)	PK/LDH assay, MDCC-PBP	1.2 ± 0.2	1.1 ± 0.1

[a]Ref. (41).

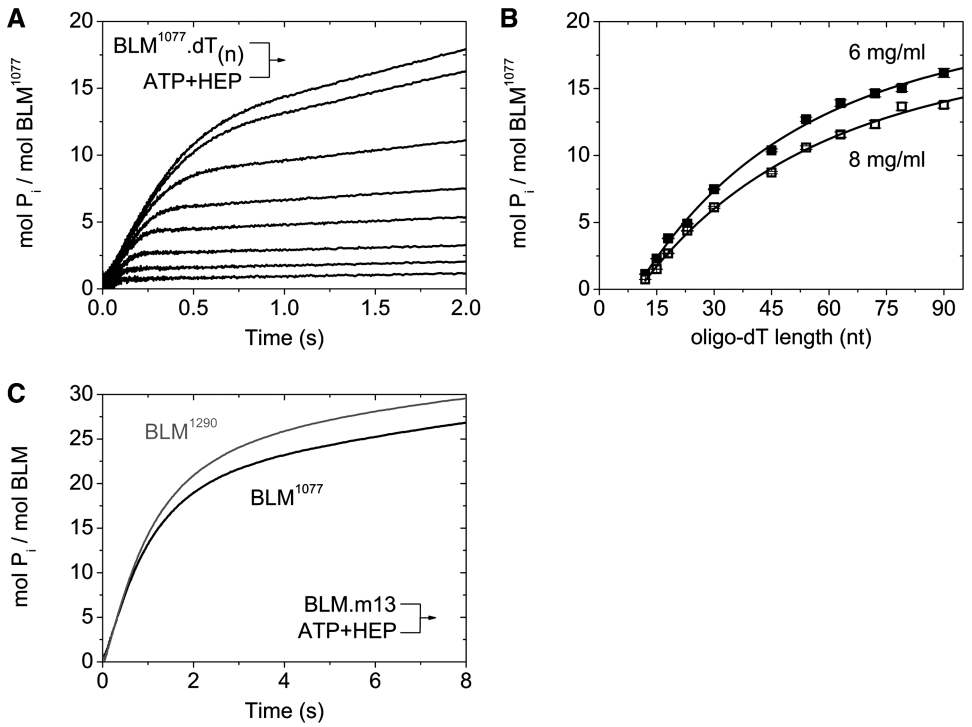

Figure 3. BLM^{1077} and BLM^{1290} translocate along ssDNA with similar mechanochemical coupling and processivity. (**A**) Transient kinetics of P_i liberation from ATP by BLM^{1077} during single-round ssDNA translocation. BLM^{1077} (0.1 μM) plus oligo-dT [1 μM, lengths (bottom to top) were 12, 15, 18, 23, 30, 45, 63 and 72 nt] was mixed with 0.5 mM ATP plus 8 mg/ml heparin (used as a protein trap) in the stopped-flow apparatus. P_i release was monitored using MDCC-PBP fluorescence (3 μM in all syringes). Fluorescence changes were converted to P_i concentration by using calibration curves. As previously described for BLM^{1290} (41,51), traces at oligo-dT lengths >12 nt consisted of an exponential burst with an amplitude of 1 mol P_i/mol BLM^{1077} (Supplementary Figure S4A), and two additional phases reflecting ATP hydrolysis during ssDNA translocation and in the trap-bound state, respectively. (**B**) Oligo-dT length dependence of the amplitudes of P_i production during the translocation phase. Data were fitted using the equation described for BLM^{1290} (41). The fit yielded translocation parameters for BLM^{1077} similar to those of BLM^{1290} (Table 1). (**C**) Transient kinetics of P_i liberation upon mixing 0.05 μM BLM^{1077} (black line) or BLM^{1290} (grey line) plus 90 μM (nt concentration) m13mp18 phage circular ssDNA with 0.5 mM ATP plus 8 mg/ml heparin in the stopped-flow apparatus. The amplitudes of P_i production during the translocation phase indicated similar mean run lengths ($\langle m \rangle$) and processivities (P) for the two constructs at the applied heparin concentration ($\langle m \rangle_{BLM1077}$ = 21 nt, $P_{BLM1077}$ = 0.955; $\langle m \rangle_{BLM1290}$ = 24 nt, $P_{BLM1290}$ = 0.961).

(C, ATP consumed/nt translocated) and processivity (P) of DNA-based motor proteins (41,51,52). Applying our previously published model (51) to the data sets showed that the coupling stoichiometry, $C = 0.83 \pm 0.11$ ATP/nt, was practically identical to that determined earlier for BLM^{1290} (Figure 3B and Table 1) (41). This value reflects that the mean step size of ~1 nt/ATP was not altered by the truncation. The processivity values of BLM^{1077} at the applied heparin concentrations (P = 0.956 and 0.951 at 6 and 8 mg/ml heparin, respectively; indicating a mean of 22 and 19 cycles taken in a single run) suggested that BLM^{1077} translocates slightly more processively along ssDNA than that reported for BLM^{1290} in similar conditions (41). To directly compare the processivities of BLM^{1077} and BLM^{1290}, we performed single-round translocation experiments with both constructs in the presence of circular m13 phage ssDNA and 8 mg/ml heparin (Figure 3C). These experiments

resulted in similar processivities for the two constructs, with a mean of 21 and 24 steps in a single run performed by BLM^{1077} and BLM^{1290}, respectively.

The WH domain harbouring the WH-pin is not necessary for DNA strand separation by BLM

The above experiments with BLM^{1077} demonstrated that the truncation of the N-terminal, WH, HRDC and C-terminal domains did not markedly affect the ATPase and ssDNA translocation properties of BLM. Next, we tested the DNA strand separation activity of BLM^{1077} on a splayed-arm DNA substrate (Figure 4A and B). Despite the fact that the WH domain [harbouring the WH-pin implicated in strand separation by RecQ1 (29,32) and WRN (31)] is entirely missing from BLM^{1077}, surprisingly we found the unwinding profile of BLM^{1077} to be similar or even slightly enhanced compared to that of BLM^{1290} (Figure 4A and B). These data demonstrate that the WH domain is not necessary for dsDNA strand separation by BLM.

BLM^{1077} is capable of annealing complementary DNA strands and disrupting D-loop structures

Synthesis-dependent strand annealing (SDSA) is one of the major routes of HR-based DNA repair in which BLM plays essential roles (Supplementary Figure S1) (1,53). In this pathway, disruption of D-loops is followed by re-annealing of the extended invading strand to the other 5′-resected end of the original DSB. To test whether these activities are retained in BLM^{1077}, we performed strand annealing (Figure 4C–F) and D-loop disruption assays (Figure 5).

We found that, at high protein concentrations, BLM^{1077} induced annealing of complementary strands, both in the absence of nucleotides and in the presence of AMPPNP (a non-hydrolysable ATP analogue), with slightly higher efficiency than BLM^{1290} (Figure 4C–F). We also performed D-loop disruption experiments in the presence of two different D-loop structures (Figure 5 and Supplementary Table S1). One substrate (3-INV) contained a 3′-invading strand with a 5′ ssDNA tail, while in the other substrate (DL) a complementary strand was annealed to the 5′ tail to rule out the possibility of D-loop unwinding based on ssDNA translocation starting from the 5′ tail. As expected based on the unaltered splayed-arm DNA unwinding activity of BLM^{1077} (Figure 4A and B), 3-INV was efficiently disrupted by this construct even at low protein concentrations (Figure 5A and C). Moreover, the DL substrate was disrupted by BLM^{1077} with the same efficiency as 3-INV (Figure 5B).

BLM^{1077} can effectively clear nucleoprotein filaments

The above results demonstrated that BLM^{1077} retains a range of DNA-based activities utilized in HR processes. We further tested the ability of BLM^{1077} to perform nucleoprotein filament displacement, an activity involving protein–protein interactions.

We measured the effect of hRad51 on the ssDNA-activated ATPase activity of BLM^{FL}, BLM^{1290} and BLM^{1077} (Figure 6A). The hRad51 concentrations required for half-maximal inhibition of the

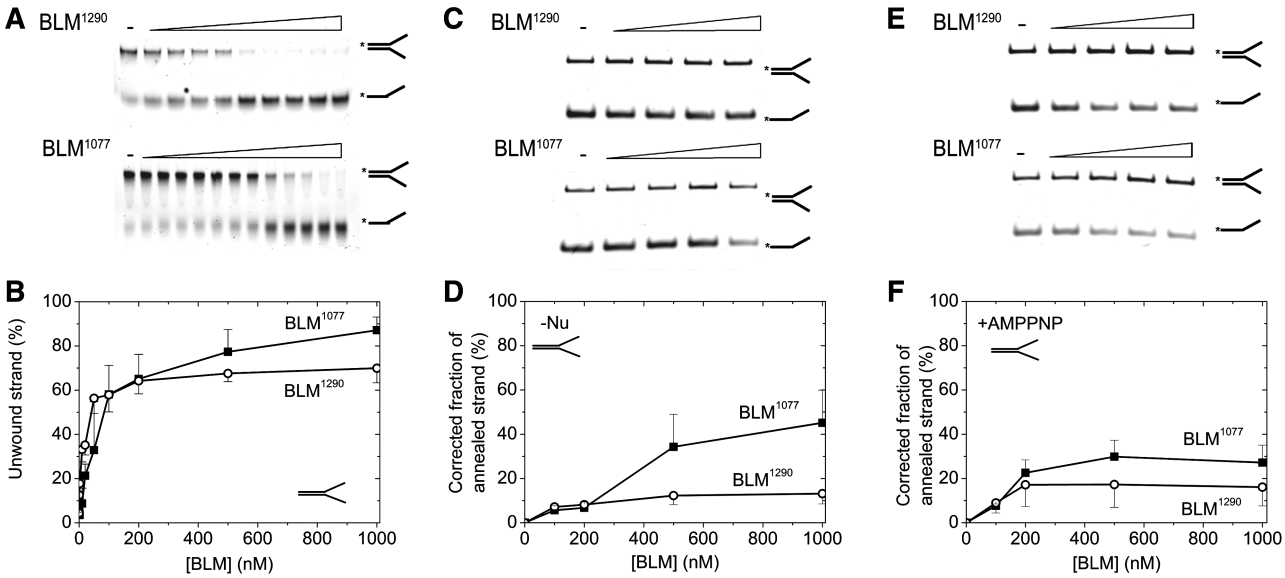

Figure 4. BLM^{1077} performs effective dsDNA unwinding and detectable strand annealing. (**A**) DNA unwinding reactions using fluorescein-labelled (asterisks) splayed-arm DNA substrate containing 33 bp of dsDNA and 21–21 nt ssDNA regions. BLM^{1077} and BLM^{1290} were incubated with the DNA substrate at different concentrations (0–1 μM) in the presence of 2 mM ATP for 15 min at 37°C. Samples were then deproteinised and run on 12% acrylamide gel. (**B**) Dependence of the extent of unwinding (%) on BLM^{1077} (filled square) and BLM^{1290} (○) concentration. Data were corrected for the fraction of ssDNA in the absence of protein. (**C–F**) Strand annealing reactions using unlabelled and fluorescein-labelled (asterisks) ssDNA substrates in the absence of nucleotides ('–Nu', **C** and **D**) and in the presence of 2 mM AMPPNP (**E** and **F**). BLM^{1077} (filled square) and BLM^{1290} (○) (0–1 μM) were incubated with the two ssDNA strands capable of forming a splayed-arm structure (identical to those in panel **A**) for 15 min at 37°C. Samples were then deproteinised and run on 12% acrylamide gel. Data were corrected for the fraction of dsDNA in the absence of protein.

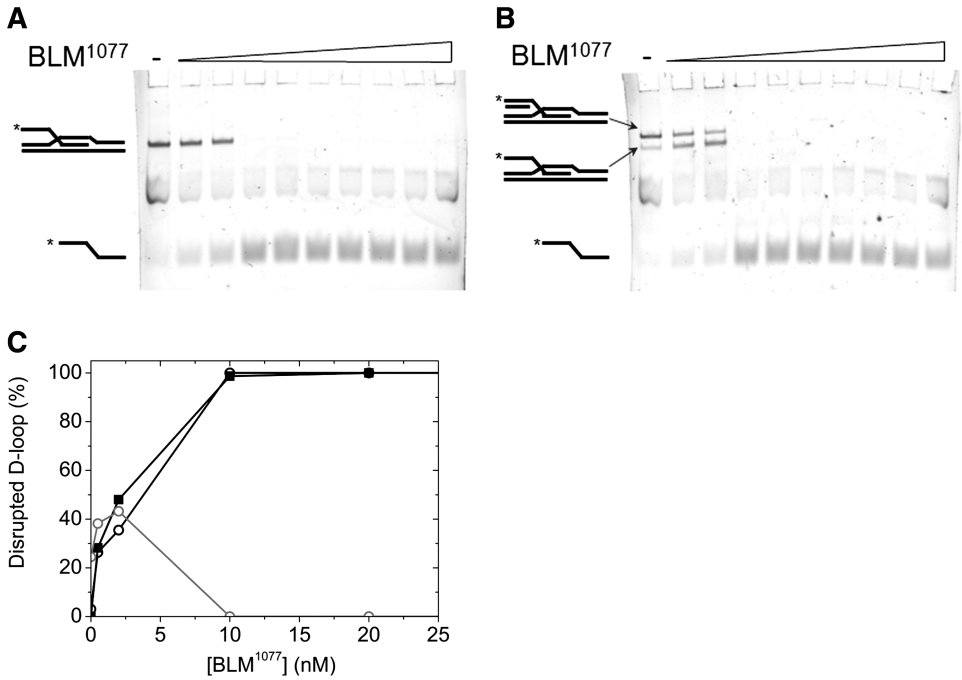

Figure 5. BLM^{1077} disrupts D-loop structures. Unwinding reactions using Cy3-labelled (asterisks) D-loop DNA substrates with a 41-nt 3′-invading strand producing 21 bp of dsDNA region and a 20-nt 5′-ssDNA tail (3-INV, **A**), or a 41-nt 3′-invading strand with a 20-nt complementary strand annealed to the 5′-ssDNA-tail (DL, **B**) (schematic representations of structures are shown). The DL sample contained 24% of 3-INV substrate (lower band, indicated), which could not be separated by chromatography. Different concentrations (0–1 μM) of BLM^{1077} were incubated with the DNA substrates for 15 min at 37°C in the presence of 2 mM ATP. Samples were then deproteinised and run on 12% acrylamide gel. (**C**) Dependence of the extent of unwinding of the labelled strand (%) on BLM^{1077} concentration. 3-INV disruption (filled square) showed similar BLM^{1077} concentration dependence to that of DL substrate (open circle). The grey plot indicates the presence of 3-INV fraction in the DL sample.

ssDNA-activated BLM ATPase were close to those expected from the stoichiometry of hRad51 binding to ssDNA [3 nt/hRad51 monomer (45)]. Interestingly, the ATPase values at saturating hRad51 concentrations remained ~20 times higher than the basal ATPase activities of each BLM construct (Figure 6A and C).

We also performed the ATPase inhibition experiments using *E. coli* SSB instead of hRad51 (Figure 6B). Similarly, to hRad51, the presence of SSB markedly decreased the ssDNA-activated ATPase activities of all three BLM constructs. However, hRad51- and SSB-inhibition significantly differed in that SSB decreased the ATPase activity of BLM^{FL} and BLM^{1290} to their basal level, while that of BLM^{1077} remained markedly higher and practically identical to that measured in the presence of hRad51 (Figure 6B and C). This finding indicates that all three BLM constructs are able to clear hRad51 filaments and, surprisingly, BLM^{1077} is also able to remove SSB from ssDNA.

Importantly, the ATPase activities reported in Figure 6A–C were calculated using the concentration of BLM molecules. However, the processes of hRad51 filament turnover and BLM-induced hRad51 clearance are also associated with ATP consumption by hRad51. The ATP turnover rate constant of ssDNA-bound hRad51 was reported to be ~0.001 s^{-1} in the absence of clearance effectors [(54), in line with our measurements]. This low activity is unlikely to significantly contribute to the observed ATP consumption rates at the applied BLM and Rad51.ssDNA concentrations. On the other hand, hRad51 clearance by BLM is likely brought about by BLM-induced enhancement of hRad51 ATPase activity, as recently described for yeast Rad51 and the Srs2 translocase (55). The ATPase rate constants reported in Figure 6A and C should therefore be viewed as those resulting from the combined action of BLM-catalysed ATP hydrolysis that drives the translocation of the helicase along ssDNA, and BLM-facilitated ATP hydrolysis by hRad51 monomers being cleared from ssDNA.

To test hRad51 nucleoprotein filament clearance more directly, we monitored this activity in stopped-flow experiments using fluorescently labelled SSB [MDCC-SSB, (47)]. When ssDNA.hRad51 or ssDNA.hRad51.BLM premixtures were rapidly mixed with MDCC-SSB in the stopped-flow apparatus, initial rapid phases of MDCC-SSB fluorescence increase were observed both in the presence and absence of ATP in the reaction (Figure 6D). These phases were therefore attributed to MDCC-SSB binding to the hRad51-free fraction of dT_{54}. In the presence of BLM constructs and ATP, a slower large increase in MDCC-SSB fluorescence was observed, reporting active hRad51 clearance from ssDNA by BLM. The kinetics and amplitude of this phase was very similar in the case of BLM^{1077}, BLM^{1290} and BLM^{FL}, indicating that all three BLM constructs are capable of hRad51 filament clearance with similar efficiencies (Figure 6D).

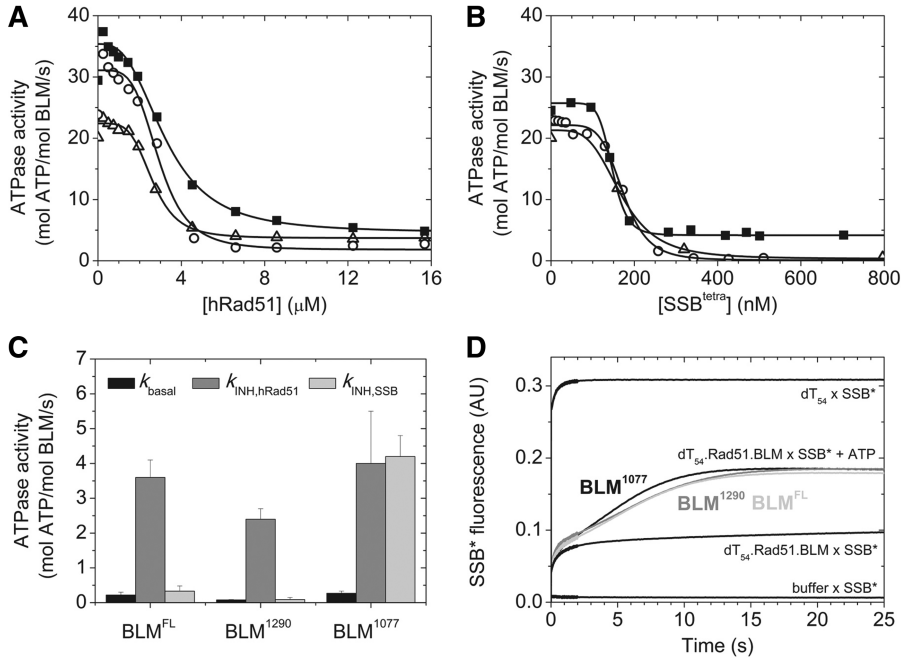

Figure 6. Nucleoprotein filament clearance by BLM constructs. (**A**) Steady-state ATPase activities of 20 nM BLM^{1077} (filled squqre), BLM^{1290} (open circle) and BLM^{FL} (open triangle) measured at 25°C in the presence of 100 nM dT_{54} and at different hRad51 concentrations. Hill-equation ($k_{ATPase} = k_0 + (k_{INH} - k_0)\frac{c_{INH}^n}{K^n + c_{INH}^n}$) was used for data fitting in which k_0 and k_{INH} are BLM ATPase activities in the absence of hRad51 and in the presence of saturating hRad51 concentration, respectively; c_{INH} is hRad51 concentration; K is the Michaelis constant and n is the cooperativity factor. Obtained values of K and n (not shown) were similar for all three constructs. (**B**) Steady-state BLM ATPase activities measured as in (**A**) except using SSB instead of hRad51. SSB tetramer concentrations are indicated. (**C**) Steady-state ATPase activities of BLM constructs in the absence of DNA (k_{basal}, black) and in the presence of saturating concentrations of hRad51 and SSB ($k_{INH,hRad51}$, grey and $k_{INH,SSB}$, light grey, respectively, cf. panels **A** and **B**). Note that $k_{INH,hRad51}$ was markedly elevated compared to k_{basal} in all three BLM constructs, indicating hRad51 filament clearance activity. Conversely, $k_{INH,SSB}$ was practically identical to k_{basal} in BLM^{FL} and BLM^{1290}, but markedly elevated in BLM^{1077}, indicating that only the latter construct is able to clear SSB from ssDNA. (**D**) Kinetics of hRad51 nucleoprotein filament clearance by BLM constructs, as monitored by MDCC-SSB fluorescence. dT_{54} (150 nM) was incubated with 2.8 μM hRad51 for 30 min on ice. BLM constructs were then added at a concentration of 200 nM, and samples were incubated for additional 10 min on ice. Traces labelled BLM^{1077} (black), BLM^{1290} (grey) and BLM^{FL} (light grey) were recorded upon rapidly mixing dT_{54}.hRad51.BLM premixtures with 1 μM MDDC-SSB (marked as SSB*) plus 2 mM ATP to monitor hRad51 clearance by BLM. The panel also shows control traces recorded upon mixing MDCC-SSB with buffer alone, MDCC-SSB with free dT_{54} (in the absence of hRad51 and BLM), and dT_{54}.Rad51.BLM premixtures with MDCC-SSB in the absence of ATP. (In the latter case, traces were very similar in the case of all BLM constructs and also when BLM was omitted.) Traces were corrected for MDCC-SSB fluorescence levels at the start of the reactions. The extent of active hRad51 clearance by BLM, as calculated from the final steady-state MDCC-SSB fluorescence levels, was 41, 41 and 39% in the case of BLM^{1077}, BLM^{1290} and BLM^{FL}, respectively.

DISCUSSION

In this study, we identified a minimal functional core region of the human BLM helicase, which is significantly shorter than previously investigated constructs showing impaired functionality (17,18,40). Our results show that the BLM core consisting of solely the two RecA domains and the ZnBD (BLM^{1077} construct) is capable of performing a multitude of mechanochemical activities utilized in DNA repair (Supplementary Figure S1) including ssDNA translocation, dsDNA unwinding, D-loop disruption and hRad51 nucleoprotein displacement. These findings demonstrate that the additional domains acquired by BLM during evolution are not required for vigorous motor activity *per se*, but play regulatory roles that may enhance the specificity and efficiency of more complex DNA-restructuring activities. For instance, in addition to its DNA binding function, the WH domain has been shown to mediate protein–protein interactions in various DNA-binding proteins. In *Fok*1 restriction endonuclease and in the 32 kDa subunit of human replication protein A (RPA), the WH domain makes little or no contact with DNA, but plays roles in protein–protein interactions (56,57). Similarly, the interaction of BLM with the FEN-1 nuclease, which is important for DNA end resection during early HR, is mediated by the RQC region of BLM (22). Available evidence suggests that, although the overall structure of the WH domain has been conserved during evolution, it has acquired versatile functions in different proteins.

The mechanistic parameters of BLM^{1077} translocation along ssDNA are highly similar to those of BLM^{1290} and BLM^{FL} (Figures 2 and 3; Supplementary Figures S3 and S4; Table 1), demonstrating that BLM^{1077} is a bona fide processive ssDNA translocase, unlike some DEAD-box RNA helicases that can unwind short stretches of dsRNA solely by kinking the RNA using the energy gained from the interaction with a single ATP molecule (58). Thus, the domains absent from BLM^{1077} do not play significant roles in ssDNA translocation.

In line with earlier studies on BLM constructs harbouring point mutations in the ZnBD (18,19,21), our results showed that the truncation of this domain impairs the folding and functioning of BLM. On the other hand, the vigorous activities of BLM^{1077} show that the presence of the WH domain, and the WH-pin located therein, is not required for efficient dsDNA unwinding by BLM. This property is in stark contrast to human RecQ1 in which the WH-pin was found essential for unwinding (29). Interestingly, BLM does not appear to harbour a characteristic pin-like structural element with an aromatic top residue in the C-core RecA domain, which could act similarly to the RecA-pin of various other helicases (Figure 1). Thus, it remains to be determined whether the BLM structural element located in this position (a charged loop (^{866}PKKPKKV^{872}) with a proline at its tip, Figure 1) can act as a DNA strand-separating pin.

BLM^{1290} was earlier shown to possess reduced DNA strand annealing capability (17), indicating that the region C-terminal from the HRDC domain is an important determinant of this property. Using higher protein concentrations, we found that BLM^{1290} was able to anneal complementary dsDNA strands, but this property was more pronounced in BLM^{1077} (Figure 4), indicating that the C-terminal region is not essential for this feature.

Besides the basic mechanochemical activities mentioned earlier, we also found that BLM^{1077} effectively unwinds D-loop structures, and the unwinding efficiency was unaffected by the presence of an 5′-ssDNA tail (Figure 5). This finding demonstrates that the core domain of BLM retains the ability to recognise and disrupt complex DNA structures encountered during HR. In complex with topoisomerase IIIα and BLAP75/RMI1, BLM^{FL} is also able to perform convergent branch migration to dissolve double Holliday junctions. Earlier truncation studies showed that the C-terminal regions missing from BLM^{1077} are essential for the dissolution activity (40), which thus appears to be the only major molecular function that cannot be performed by the minimal motor core of BLM.

One of the most important roles of BLM during HR is quality control, which is brought about by its capability to disrupt hRad51 nucleoprotein filaments (Supplementary Figure S1) (6). This activity is indispensable to avoid illegitimate HR events in mitotic cells, which could otherwise lead to chromosome rearrangements and cancerous processes. Consequently, a characteristic feature of Bloom's syndrome patients and cell lines is the elevated frequency of sister chromatid exchange events (59). Nucleoprotein filament disassembly is based on ssDNA translocation and acceleration of hRad51 dissociation from ssDNA by BLM (6). Based on results on yeast Rad51 and Srs2 helicase (55), it appears likely that BLM accelerates the ATPase activity of hRad51, which leads to the weakening of the hRad51-DNA interaction and, in turn, the dissociation of hRad51 from ssDNA. We found that BLM^{1077} is capable of clearing hRad51 nucleoprotein filaments with the same efficiency as BLM^{1290} and BLM^{FL} (Figure 6A, C and D). Surprisingly, the ATPase profiles of BLM^{1077} in the presence of bacterial SSB filaments indicated that this construct is even able to dismantle SSB from ssDNA, unlike the longer BLM constructs (Figure 6B). This result suggests that the RecA-ZnBD core of BLM is a vigorous ssDNA translocase, and the additional domains may not only confer more complex functions but may also negatively regulate mechanochemical activities.

SUPPLEMENTARY DATA

Supplementary Data are available at NAR Online: Supplementary Table 1, Supplementary Figures 1–4 and pdb files of BLM homology models (BLM_1OYY.pdb and BLM_2WWY.pdb).

FUNDING

Norway Grants (NNF2-85613 to M.K.); Hungarian Scientific Research Fund (K71915 and NK81950 to M.K.); TÁMOP Grant (4.2.1/B-09/1/KMR-2010-0003 to M.K.); Human Frontier Science Program (RGY0072/2010 to M.K.) and 'Momentum' Program of the Hungarian Academy of Sciences (LP2011-006/2011 to M.K.). M.K. is a Bolyai Fellow of the Hungarian Academy of Sciences. Funding for open access charge: Momentum' Program of the Hungarian Academy of Sciences (LP2011-006/2011 to M.K.).

Conflict of interest statement. None declared.

REFERENCES

1. Chu,W.K. and Hickson,I.D. (2009) RecQ helicases: multifunctional genome caretakers. *Nat. Rev. Cancer*, **9**, 644–654.
2. Bachrati,C.Z. and Hickson,I.D. (2008) RecQ helicases: guardian angels of the DNA replication fork. *Chromosoma*, **117**, 219–233.
3. Nimonkar,A.V., Genschel,J., Kinoshita,E., Polaczek,P., Campbell,J.L., Wyman,C., Modrich,P. and Kowalczykowski,S.C. (2011) BLM-DNA2-RPA-MRN and EXO1-BLM-RPA-MRN constitute two DNA end resection machineries for human DNA break repair. *Genes Dev.*, **25**, 350–362.
4. Gravel,S., Chapman,J.R., Magill,C. and Jackson,S.P. (2008) DNA helicases Sgs1 and BLM promote DNA double-strand break resection. *Genes Dev.*, **22**, 2767–2772.
5. Bugreev,D.V., Mazina,O.M. and Mazin,A.V. (2009) Bloom syndrome helicase stimulates RAD51 DNA strand exchange activity through a novel mechanism. *J. Biol. Chem.*, **284**, 26349–26359.
6. Bugreev,D.V., Yu,X., Egelman,E.H. and Mazin,A.V. (2007) Novel pro- and anti-recombination activities of the Bloom's syndrome helicase. *Genes Dev.*, **21**, 3085–3094.
7. Chu,W.K., Hanada,K., Kanaar,R. and Hickson,I.D. (2010) BLM has early and late functions in homologous recombination repair in mouse embryonic stem cells. *Oncogene*, **29**, 4705–4714.
8. Karow,J.K., Newman,R.H., Freemont,P.S. and Hickson,I.D. (1999) Oligomeric ring structure of the Bloom's syndrome helicase. *Curr. Biol.*, **9**, 597–600.
9. Beresten,S.F., Stan,R., van Brabant,A.J., Ye,T., Naureckiene,S. and Ellis,N.A. (1999) Purification of overexpressed hexahistidine-tagged BLM N431 as oligomeric complexes. *Protein Expr. Purif.*, **17**, 239–248.
10. Bergeron,K.L., Murphy,E.L., Brown,L.W. and Almeida,K.H. (2011) Critical interaction domains between bloom syndrome protein and RAD51. *Protein J.*, **30**, 1–8.

11. Brosh,R.M. Jr, Li,J.L., Kenny,M.K., Karow,J.K., Cooper,M.P., Kureekattil,R.P., Hickson,I.D. and Bohr,V.A. (2000) Replication protein A physically interacts with the Bloom's syndrome protein and stimulates its helicase activity. *J. Biol. Chem.*, **275**, 23500–23508.
12. Singh,T.R., Ali,A.M., Busygina,V., Raynard,S., Fan,Q., Du,C.H., Andreassen,P.R., Sung,P. and Meetei,A.R. (2008) BLAP18/RMI2, a novel OB-fold-containing protein, is an essential component of the Bloom helicase-double Holliday junction dissolvasome. *Genes Dev.*, **22**, 2856–2868.
13. Wu,L., Bachrati,C.Z., Ou,J., Xu,C., Yin,J., Chang,M., Wang,W., Li,L., Brown,G.W. and Hickson,I.D. (2006) BLAP75/RMI1 promotes the BLM-dependent dissolution of homologous recombination intermediates. *Proc. Natl Acad. Sci. USA*, **103**, 4068–4073.
14. Wu,L., Davies,S.L., Levitt,N.C. and Hickson,I.D. (2001) Potential role for the BLM helicase in recombinational repair via a conserved interaction with RAD51. *J. Biol. Chem.*, **276**, 19375–19381.
15. Wu,L., Davies,S.L., North,P.S., Goulaouic,H., Riou,J.F., Turley,H., Gatter,K.C. and Hickson,I.D. (2000) The Bloom's syndrome gene product interacts with topoisomerase III. *J. Biol. Chem.*, **275**, 9636–9644.
16. Wu,L. and Hickson,I.D. (2003) The Bloom's syndrome helicase suppresses crossing over during homologous recombination. *Nature*, **426**, 870–874.
17. Cheok,C.F., Wu,L., Garcia,P.L., Janscak,P. and Hickson,I.D. (2005) The Bloom's syndrome helicase promotes the annealing of complementary single-stranded DNA. *Nucleic Acids Res.*, **33**, 3932–3941.
18. Janscak,P., Garcia,P.L., Hamburger,F., Makuta,Y., Shiraishi,K., Imai,Y., Ikeda,H. and Bickle,T.A. (2003) Characterization and mutational analysis of the RecQ core of the bloom syndrome protein. *J. Mol. Biol.*, **330**, 29–42.
19. Guo,R.B., Rigolet,P., Zargarian,L., Fermandjian,S. and Xi,X.G. (2005) Structural and functional characterizations reveal the importance of a zinc binding domain in Bloom's syndrome helicase. *Nucleic Acids Res.*, **33**, 3109–3124.
20. Huber,M.D., Duquette,M.L., Shiels,J.C. and Maizels,N. (2006) A conserved G4 DNA binding domain in RecQ family helicases. *J. Mol. Biol.*, **358**, 1071–1080.
21. Neff,N.F., Ellis,N.A., Ye,T.Z., Noonan,J., Huang,K., Sanz,M. and Proytcheva,M. (1999) The DNA helicase activity of BLM is necessary for the correction of the genomic instability of bloom syndrome cells. *Mol. Biol. Cell*, **10**, 665–676.
22. Sharma,S., Sommers,J.A., Wu,L., Bohr,V.A., Hickson,I.D. and Brosh,R.M. Jr (2004) Stimulation of flap endonuclease-1 by the Bloom's syndrome protein. *J. Biol. Chem.*, **279**, 9847–9856.
23. Velankar,S.S., Soultanas,P., Dillingham,M.S., Subramanya,H.S. and Wigley,D.B. (1999) Crystal structures of complexes of PcrA DNA helicase with a DNA substrate indicate an inchworm mechanism. *Cell*, **97**, 75–84.
24. Korolev,S., Hsieh,J., Gauss,G.H., Lohman,T.M. and Waksman,G. (1997) Major domain swiveling revealed by the crystal structures of complexes of E. coli Rep helicase bound to single-stranded DNA and ADP. *Cell*, **90**, 635–647.
25. Lee,J.Y. and Yang,W. (2006) UvrD helicase unwinds DNA one base pair at a time by a two-part power stroke. *Cell*, **127**, 1349–1360.
26. Buttner,K., Nehring,S. and Hopfner,K.P. (2007) Structural basis for DNA duplex separation by a superfamily-2 helicase. *Nat. Struct. Mol. Biol.*, **14**, 647–652.
27. Saikrishnan,K., Powell,B., Cook,N.J., Webb,M.R. and Wigley,D.B. (2009) Mechanistic basis of 5′-3′ translocation in SF1B helicases. *Cell*, **137**, 849–859.
28. Bernstein,D.A., Zittel,M.C. and Keck,J.L. (2003) High-resolution structure of the E.coli RecQ helicase catalytic core. *EMBO J.*, **22**, 4910–4921.
29. Pike,A.C., Shrestha,B., Popuri,V., Burgess-Brown,N., Muzzolini,L., Costantini,S., Vindigni,A. and Gileadi,O. (2009) Structure of the human RECQ1 helicase reveals a putative strand-separation pin. *Proc. Natl Acad. Sci. USA*, **106**, 1039–1044.
30. German,J., Sanz,M.M., Ciocci,S., Ye,T.Z. and Ellis,N.A. (2007) Syndrome-causing mutations of the BLM gene in persons in the Bloom's Syndrome Registry. *Hum. Mutat.*, **28**, 743–753.
31. Kitano,K., Kim,S.Y. and Hakoshima,T. (2010) Structural basis for DNA strand separation by the unconventional winged-helix domain of RecQ helicase WRN. *Structure*, **18**, 177–187.
32. Lucic,B., Zhang,Y., King,O., Mendoza-Maldonado,R., Berti,M., Niesen,F.H., Burgess-Brown,N.A., Pike,A.C., Cooper,C.D., Gileadi,O. *et al.* (2011) A prominent beta-hairpin structure in the winged-helix domain of RECQ1 is required for DNA unwinding and oligomer formation. *Nucleic Acids Res.*, **39**, 1703–1717.
33. Bernstein,D.A. and Keck,J.L. (2003) Domain mapping of Escherichia coli RecQ defines the roles of conserved N- and C-terminal regions in the RecQ family. *Nucleic Acids Res*, **31**, 2778–2785.
34. Bernstein,D.A. and Keck,J.L. (2005) Conferring substrate specificity to DNA helicases: role of the RecQ HRDC domain. *Structure*, **13**, 1173–1182.
35. Ozsoy,A.Z., Sekelsky,J.J. and Matson,S.W. (2001) Biochemical characterization of the small isoform of Drosophila melanogaster RECQ5 helicase. *Nucleic Acids Res.*, **29**, 2986–2993.
36. Muzzolini,L., Beuron,F., Patwardhan,A., Popuri,V., Cui,S., Niccolini,B., Rappas,M., Freemont,P.S. and Vindigni,A. (2007) Different quaternary structures of human RECQ1 are associated with its dual enzymatic activity. *PLoS Biol.*, **5**, e20.
37. Bennett,R.J., Sharp,J.A. and Wang,J.C. (1998) Purification and characterization of the Sgs1 DNA helicase activity of *Saccharomyces cerevisiae*. *J. Biol. Chem.*, **273**, 9644–9650.
38. Kobbe,D., Blanck,S., Focke,M. and Puchta,H. (2009) Biochemical characterization of AtRECQ3 reveals significant differences relative to other RecQ helicases. *Plant Physiol.*, **151**, 1658–1666.
39. Hartung,F. and Puchta,H. (2006) The RecQ gene family in plants. *J. Plant. Physiol.*, **163**, 287–296.
40. Wu,L., Chan,K.L., Ralf,C., Bernstein,D.A., Garcia,P.L., Bohr,V.A., Vindigni,A., Janscak,P., Keck,J.L. and Hickson,I.D. (2005) The HRDC domain of BLM is required for the dissolution of double Holliday junctions. *EMBO J.*, **24**, 2679–2687.
41. Gyimesi,M., Sarlos,K. and Kovacs,M. (2010) Processive translocation mechanism of the human Bloom's syndrome helicase along single-stranded DNA. *Nucleic Acids Res.*, **38**, 4404–4414.
42. Sambrook,J. and Russel,D.W. (2001) *Molecular Cloning*, 3rd edn. Cold Spring Harbor Laboratory Press, Cold Spring Harbor, NY, USA.
43. Karow,J.K., Chakraverty,R.K. and Hickson,I.D. (1997) The Bloom's syndrome gene product is a 3′—5′ DNA helicase. *J. Biol. Chem.*, **272**, 30611–30614.
44. Brune,M., Hunter,J.L., Corrie,J.E. and Webb,M.R. (1994) Direct, real-time measurement of rapid inorganic phosphate release using a novel fluorescent probe and its application to actomyosin subfragment 1 ATPase. *Biochemistry*, **33**, 8262–8271.
45. Sigurdsson,S., Trujillo,K., Song,B., Stratton,S. and Sung,P. (2001) Basis for avid homologous DNA strand exchange by human Rad51 and RPA. *J. Biol. Chem.*, **276**, 8798–8806.
46. Lohman,T.M., Green,J.M. and Beyer,R.S. (1986) Large-scale overproduction and rapid purification of the Escherichia coli ssb gene product. Expression of the ssb gene under lambda PL control. *Biochemistry*, **25**, 21–25.
47. Dillingham,M.S., Tibbles,K.L., Hunter,J.L., Bell,J.C., Kowalczykowski,S.C. and Webb,M.R. (2008) Fluorescent single-stranded DNA binding protein as a probe for sensitive, real-time assays of helicase activity. *Biophys. J.*, **95**, 3330–3339.
48. Shatsky,M., Dror,O., Schneidman-Duhovny,D., Nussinov,R. and Wolfson,H.J. (2004) BioInfo3D: a suite of tools for structural bioinformatics. *Nucleic Acids Res*, **32**, W503–W507.
49. Sali,A. and Blundell,T.L. (1993) Comparative protein modelling by satisfaction of spatial restraints. *J. Mol. Biol.*, **234**, 779–815.
50. Laskowski,R.A., MacArthur,M.W., Moss,D.S. and Thorthon,J.M. (1993) PROCHECK: a program to check the stereochemical quality of protein structures. *J. Appl. Cryst.*, **26**, 283–291.
51. Gyimesi,M., Sarlos,K., Derenyi,I. and Kovacs,M. (2010) Streamlined determination of processive run length and

mechanochemical coupling of nucleic acid motor activities. *Nucleic Acids Res.*, **38**, e102.
52. Tomko,E.J., Fischer,C.J., Niedziela-Majka,A. and Lohman,T.M. (2007) A nonuniform stepping mechanism for E. coli UvrD monomer translocation along single-stranded DNA. *Mol. Cell*, **26**, 335–347.
53. Adams,M.D., McVey,M. and Sekelsky,J.J. (2003) Drosophila BLM in double-strand break repair by synthesis-dependent strand annealing. *Science*, **299**, 265–267.
54. Chi,P., Van Komen,S., Sehorn,M.G., Sigurdsson,S. and Sung,P. (2006) Roles of ATP binding and ATP hydrolysis in human Rad51 recombinase function. *DNA Repair (Amst)*, **5**, 381–391.
55. Antony,E., Tomko,E.J., Xiao,Q., Krejci,L., Lohman,T.M. and Ellenberger,T. (2009) Srs2 disassembles Rad51 filaments by a protein-protein interaction triggering ATP turnover and dissociation of Rad51 from DNA. *Mol. Cell*, **35**, 105–115.
56. Wah,D.A., Hirsch,J.A., Dorner,L.F., Schildkraut,I. and Aggarwal,A.K. (1997) Structure of the multimodular endonuclease FokI bound to DNA. *Nature*, **388**, 97–100.
57. Deng,X., Habel,J.E., Kabaleeswaran,V., Snell,E.H., Wold,M.S. and Borgstahl,G.E. (2007) Structure of the full-length human RPA14/32 complex gives insights into the mechanism of DNA binding and complex formation. *J. Mol. Biol.*, **374**, 865–876.
58. Pyle,A.M. (2008) Translocation and unwinding mechanisms of RNA and DNA helicases. *Annu. Rev. Biophys.*, **37**, 317–336.
59. Chaganti,R.S., Schonberg,S. and German,J. (1974) A manyfold increase in sister chromatid exchanges in Bloom's syndrome lymphocytes. *Proc. Natl Acad. Sci. USA*, **71**, 4508–4512.